ELSEVIER

Contents lists available at ScienceDirect

BBA - Biomembranes

journal homepage: www.elsevier.com/locate/bbamem





Cells immersed in collagen matrices show a decrease in plasma membrane fluidity as the matrix stiffness increases

Joao Aguilar ^a, Leonel Malacrida ^{b,c}, German Gunther ^d, Belén Torrado ^e, Viviana Torres ^f, Bruno F. Urbano ^a, Susana A. Sánchez ^{a,*}

- a Laboratorio de Interacciones Macromoleculares (LIMM), Departamento de Polímeros, Facultad de Ciencias Químicas, Universidad de Concepción, Concepción, Chile
- ^b Departamento de Fisiopatología, Hospital de Clínicas, Universidad de la República, Montevideo, Uruguay
- ^c Advanced Bioimaging Unit, Institut Pasteur Montevideo, Universidad de la República, Montevideo, Uruguay
- ^d Facultad de Ciencias Químicas y Farmacéuticas, Universidad de Chile, Santiago, Chile
- ^e Biomedical Engineering Department, University of California at Irvine, California, USA
- f Departamento de Bioquímica, Facultad de Ciencias Biológicas, Universidad de Concepción, Concepción, Chile

ARTICLE INFO

Keywords: Membrane heterogeneity Spectral phasor analysis LAURDAN Membrane fluidity Collagen matrices Extracellular stiffness

ABSTRACT

Cells are constantly adapting to maintain their identity in response to the surrounding media's temporal and spatial heterogeneity. The plasma membrane, which participates in the transduction of external signals, plays a crucial role in this adaptation. Studies suggest that nano and micrometer areas with different fluidities at the plasma membrane change their distribution in response to external mechanical signals. However, investigations linking fluidity domains with mechanical stimuli, specifically matrix stiffness, are still in progress. This report tests the hypothesis that the stiffness of the extracellular matrix can modify the equilibrium of areas with different order in the plasma membrane, resulting in changes in overall membrane fluidity distribution. We studied the effect of matrix stiffness on the distribution of membrane lipid domains in NIH-3 T3 cells immersed in matrices of varying concentrations of collagen type I, for 24 or 72 h. The stiffness and viscoelastic properties of the collagen matrices were characterized by rheometry, fiber sizes were measured by Scanning Electron Microscopy (SEM) and the volume occupied by the fibers by second harmonic generation imaging (SHG). Membrane fluidity was measured using the fluorescent dye LAURDAN and spectral phasor analysis. The results demonstrate that an increase in collagen stiffness alters the distribution of membrane fluidity, leading to an increasing amount of the LAURDAN fraction with a high degree of packing. These findings suggest that changes in the equilibrium of fluidity domains could represent a versatile and refined component of the signal transduction mechanism for cells to respond to the highly heterogeneous matrix structural composition. Overall, this study sheds light on the importance of the plasma membrane's role in adapting to the extracellular matrix's mechanical cues.

1. Introduction

Cells in vivo are surrounded by extracellular media (ECM) and they must develop strategies to adapt to structural and temporal changes experienced by the ECM. At the same time, the ECM is also modified by the cell. This cell-ECM adaptation occurs in normal processes such as embryogenesis, wound healing, and angiogenesis. Any impairment in these processes may give rise to different conditions such as, fibrosis, lung disorders, inflammation etc., [1] or lead to diseases such as atherosclerosis and cancer among others [2,3]. The importance of cell-

ECM interactions is well accepted today, yet most of the cellular studies in the literature are performed in culture dishes using a liquid culture media, a methodology established by Ross Granville Harrison in 1907 [4], indicating that these interactions have been ignored for a long time. Today, it is generally accepted that two parameters are missed in the monolayer cell culturing methodology: 3D cell spatial configuration and media stiffness [5]. Indeed, cells in vivo are part of a 3D topology defined by the extracellular matrix (ECM) presenting some degree of viscosity (plasma), fibrous netting (extracellular matrix) or diverse porosity (bones). The interactions between cell and ECM significantly

E-mail address: susanchez@udec.cl (S.A. Sánchez).

^{*} Corresponding author at: Laboratorio de Interacciones Macromoleculares (LIMM), Departamento de Polímeros, Facultad de Ciencias Químicas, Universidad de Concepción, Edmundo Larenas 129, Concepción, Chile.

differ from the ones existing in the monolayer model, since cells are not only exposed to chemical but also to mechanical stimulus. Mechanical stimulus in vivo arises from hydrostatic changes [6], extracellular vascular shear stress [7], osmolality changes and ECM stiffness [8] and they are heterogeneous in magnitude, frequency and duration [7]. Using 3D ECM models (matrices, spheroids, scaffolds etc.) [5] researchers have demonstrated that besides the main role of the ECM to protect and support the cells, it is a mechanical stimulus for several biological processes [9]. However, the details of sensing and translation of this type of stimulus is still under investigation. Several parameters of the ECM (forces, deformations, geometry, and stiffness) activate cellular functions [8]. In fact, ECM stiffness can deeply influence development, homeostasis, disease progression and cell behavior [9] by affecting process such as: stem cell fate [10,11], cell migration [12], differentiation [13], cell spreading [14], orientation [15] and contractility [16].

1.1. Lipid domains distribution: a mechanism for membrane participation in signal transduction

The role of the plasma membrane in cell signaling is proposed to require membrane domains or rafts. Rafts would be involved in localizing the required components within a membrane compartment, assembling, and disassembling facilitating protein sequestering and release, and amplifying and modulating the signals by coalescence of one or more types of lipid rafts [17–21]. This model is well supported in the translation of chemical stimulus [19,22,23] and changes in the distribution of rafts would be the mechanism by which they act as platforms for local activation and coordination of signaling [24–26]. The participation of the plasma membrane in mechanical signal transduction is not totally understood, but the participation of lipid domains is postulated: (a) Ross et all [27] reported the involvement of conformational changes on the integrin family of proteins in the translation of force and tension stimulus, (b) Caveolin 1 (Cav-1), a protein localized in caveolae, a particular type of lipid raft, was found to mediate differentiation of lung epithelial cells induced by mechanical force [28], migration of endothelial cells [29] and regulation of vessel diameter by shear stress [30], (c) reciprocal auto regulation of Cav-1 and Beta-1 Integrin is shown to be influenced by matrix stiffness [31], (d) Raft content correlated with the extent of cell membrane deformation [32] and (e) mechanical disruption of the rafts activate enzymatic activity by releasing the enzyme from the raft [33]. The mechanism of changes in lipid domains distribution in the translation of mechanical signaling is also supported by the literature: (a) electric field directs cell migration and proliferation by inducing accumulation (coalescence) of rafts [34] and partition of integrin and Cav-1 [35], (b) rapid caveolae disassembly and slow reassembly is reported as a response to rapid changes in membrane tension [36]. A small number of biophysical studies support this model: Yamamoto et al., using LAURDAN Generalized Polarization reported that plasma membranes respond to mechanical stimulus such a stretch and shear stress by changing fluidity, lipid order and cholesterol content [37]. They showed that membrane response is different for these two stimuli: uniaxial stretching and hypotonic swelling increased while shear stress decreased the order of the plasma membrane [38]. This opposite response led them to conclude that membrane physical properties are involved in mechano-transduction activating membrane receptors specific to each force [37,39].

1.2. LAURDAN spectral properties and the spectral phasor analysis: a technique to study lipid domains dynamics [40–42]

This technique measures membrane heterogeneity by analyzing the emission spectral shift of LAURDAN (6-lauroyl,1-2-dimethylamino naphthalene) using the phasor analysis of spectral images [43]. LAURDAN is a fluorescent probe that has been used to study polarity and dipolar relaxation in membranes [44]. When LAURDAN is excited, its dipole moment is increased, which can reorient surrounding dipoles in

the environment, and this process requires solvent molecules to move within the excited state lifetime of LAURDAN [45]. The red shift of LAURDAN fluorescence reflects the amount of energy utilized in the process of environment reorganization [46]. LAURDAN can detect changes in the physical state of the membrane, determined by the fatty acid composition and thermodynamic condition. LAURDAN fluorescence emission is centered at 440 nm for gel and liquid order membranes, and is red-shifted 50 nm for liquid disorder membranes [47]. LAURDAN senses confined molecules of water that cannot freely rotate at the membrane interphase [48]. Also, LAURDAN is sensitive to cholesterol concentration, which modifies the membrane order parameters [49,50].

Spectral phasor analysis has been applied to biological systems [41,43,44,51] and has the advantage of providing information about complex interactions such as the ones present in the LAURDAN/membrane system, simplifying the understanding of complex interactions [44]. This technique has been shown to be an excellent tool for the study of membrane fluidity heterogeneity with high spatial resolution in living cells [41,51,52].

We hypothesize that plasma membrane fluidity is the result of a distribution of areas with different order in equilibrium with each other, and fluidity changes are the results of a modification of this equilibrium and a redistribution of the areas. In this report we studied the changes in membrane heterogeneity in cells immersed in collagen matrices of different stiffness. The characterization of the collagen matrices was done by rheometry (viscoelastic properties) by scanning electron microscopy (fiber size) and reversed second harmonic generation (SHG) signal (volume occupied by the fibers). To analyze the distribution of membrane fluidity in natural membranes phasor analysis of LAURDAN spectral images was used [43]. This methodology joins the fast spectral image acquisition and the power of the phasor analysis for images and have been showed to be an excellent tool to study membrane fluidity changes [43,44,53,54]. It is important to mention that the resolution of the images analyzed by the spectral phasor approach are diffractionlimited (dependent on the two-photon microscope used), and therefore does not allow one to observe the nanometric lipid domains postulated to exist on natural membranes [22], rather it measures micrometric areas resulting from the coalescence of nano domains and more fluid areas [20,41,42,44].

2. Experimental

2.1. Collagen matrices with variable stiffness

2.1.1. Matrices fabrication.

Collagen matrices having different stiffness were prepared using different concentrations of collagen and the method of gelation by temperature [55]. A stock solution of collagen type-I 5 mg/mL in acetic acid (Gibco, USA) was used to prepare collagen solutions with concentrations 0.5, 1.0, 2.0 and 4.0 mg/mL. The solutions were prepared by mixing the appropriate amounts of the stock collagen, PBS $10\times$ (100 μL for a 1 mL preparation) and DMEM (Dulbecco's Modified Eagle Medium, Thermo Fisher, USA). Individual reagents and the mixture were kept on ice to avoid gelation during the process. After mixing, the pH of each mixture was raised to neutral pH by adding NaOH 0.5 mol/L. The pH changes were monitored following the color changes of the phenol red present in the DMEM media, a useful strategy to work with small volumes. A very gentle vortexing was used to prepare the mixture. Finally, the matrices were formed by incubation at 37 °C in 8 well imaging dishes. Two incubation times were used, namely 24 and 72 h.

2.1.2. Matrices characterization

2.1.2.1. Fiber diameter. Fiber diameters were measured from scanning electron microscopy (SEM) images obtained in a SEM-PROBE CAMECA

model SU-30. For sample preparation, after gelation, the matrices were fixed by incubating them in 2.5 % formaldehyde for 1 day at 4 °C. Later the samples were dried using the methodology of alcohol dehydration. In this methodology the fixed samples are first rinsed with phosphate buffer and then the sample is incubated for 40 min in ethanol/water solutions of concentrations of 10, 20, 30, 40, 50, 70, 80, 90 and 100 %. After the last concentrated ethanol the sample is dried by evaporation of the ethanol [56]. For the SEM imaging, the samples were covered by gold. For each collagen concentration, images of 6.40 \times 4.80 μ m (1280 \times 960 pixels) at 4 different positions were analyzed. A total of 80 individual fibers were measured to calculate the average fiber size for each collagen concentration, using standard tools from Image J software1.53 s.

Volume fraction occupied by the fibers. Matrices of different collagen concentration were fixed by incubating them in 2.5 % formaldehyde for 1 day at 4 °C and rinsing with phosphate buffer. Second harmonic generation intensity and lifetime signals in several z planes were obtained using a noncommercial microscope designed for deep tissue imaging [57]. The phasor analysis for fluorescence lifetime imaging microscopy (FLIM) analysis is based on the transformation of the fluorescence decay histogram I(t) into its sine and cosine components [58]. Data are displayed in a polar plot (phasor plot) with coordinates S = M $\cos \phi$ and $G = M \sin \phi$, with ϕ being the phase delay and M the demodulation between excitation and emission [59,60]. In the phasor representation, a point (phasor), with S and G coordinates, represents each fluorescent species involved. In an image, the lifetime will be determined at each pixel and its corresponding phasor will be located on the phasor plot. Thus, the phasor plot contains as many phasors as the number of pixels acquired in the image. Pure fluorescent species (with single exponential decay) will lie on the phasor representation on what is known as the universal circle (shown with a semicircle). For the analysis, a color cursor (red) on the phasor plot was used to label the pixels in the original intensity image from where the phasors from collagen originated. These images and standard tools from Image J software were used to calculate first the area occupied by collagen at each image of the z-stack and second the volume occupied by collagen by adding the areas of each image on the z-stack. For each collagen concentration, four stacks of 11 images ($30 \times 30 \times 2 = 1800 \, \mu \text{m}^3$) were measured, averaged, and the standard deviation was determined.

2.1.2.2. Viscoelastic properties. The viscoelastic properties of the collagen gels were studied by rheometry using a DHR-3, TA Instrument implemented with parallel plates and a Peltier plate for temperature control. Oscillatory amplitude tests were performed using geometry of 8 mm, a 1 mm gap, a deformation range from 0.01 to 100 %, at a temperature of 37 °C. From this test, the linear viscoelastic region, storage modulus (G'), loss modulus (G'') were measured and the complex modulus (G^*) calculated using the following equation:

$$G^* = \sqrt{G^{'2} + G^{''2}}$$

2.1.3. Cells culture

Cells grow in the collagen matrices and LAURDAN staining.

NIH 3 T3 (ATCC CRL-1658) mouse fibroblasts were growth using already published protocols [46]. Briefly, cells were grown in DMEM media at 37 °C and 5 % CO $_2$ in culture plates. After incubation cells were rinsed with PBS, detached with trypsin, and neutralized with fetal bovine serum. The final cell concentration was $\sim\!\!6\times10^6$ cells/mL. To prepare the NIH 3 T3 embedded on the collagen, an aliquot from the stock cell culture was added to 1 mL of collagen solution to reach a cell concentration of 100,000 cell/mL. Then, 300 μ L of this mixture were deposited in the wells of an 8 wells chamber with optical glass (MATTEK, USA). After incubation of the chambers for 40 min at 37 °C and 5 % CO $_2$ culture media was added to each chamber to avoid sample drying and then they were incubated for either 24 or 72 h. Every 24 h the media was replaced by fresh media having LAURDAN 1 μ mol/L.

Cell viability assay. Cell viability of NIH 3 T3 cells in collagen at different concentrations was tested using Sytox Orange (Thermo Fischer Scientific, USA) and NucRedLive 647 (Termo Fischer scientific, USA) to label the nucleus of dead and alive cells in culture, respectively. NIH 3 T3 cells were labeled according to vendor protocol and 5 \times 5 tile images of 2124 \times 2124 pixels were obtained. Images were registered in a Confocal Zeiss 710 NLO using an excitation wavelength of 488 or 633 nm and emission ranges of 503–579 and 659–740 nm for Sytox Orange and NucRedLive 647, respectively. In the analysis green (dead) and red (alive) cells were quantified, and the viability percentage was obtained for each collagen concentration. All measurements were done at 37 $^{\circ}\mathrm{C}.$

2.1.4. LAURDAN hyperspectral imaging and spectral phasor analysis

Hyperspectral images were obtained in a confocal scanning microscope Zeiss 710NLO equipped with a spectral detector of 32 channels. A Ti:Sapphire laser (Spectra-Physics Mai Tai) with 80 MHz repetition rate tuned at 780 nm was used to excite the sample. The length of the spectrum used for the spectral images was 415–726 nm, with 10 nm steps. Spectral images were acquired with a pixel dwell time of 1.58 μs , and with a resolution of 515 \times 512 pixels. For all images the pixel size was fixed at 100 mn. The objective used for all the spectral images was a Zeiss C-Apochromat 40×/1.2w KorrM27. Spectral images were Fourier transformed (using the first harmonic) to the phasor coordinates using the SimFCS software (G-Soft, Global for Images, Urbana-Illinois, USA) as described previously [43,44].

In a spectral image, each pixel contains the emission spectrum at that pixel. Therefore, an emission curve is associated with every pixel. The spectral image can be analyzed in a global manner using the phasor approach. Spectral phasor analysis [44,61,62] is based on the transformation of the emission spectra into a phasor by calculating the Fourier real and imaginary component as coordinates G (cosine transform) and S (sine transform) according to the following mathematical expressions:

$$X = G = \frac{\sum_{\lambda} I(\lambda) cos(2\pi n\lambda/L)}{\sum_{\lambda} I(\lambda)} \text{ and } Y = S = \frac{\sum_{\lambda} I(\lambda) sin(2\pi n\lambda/L)}{\sum_{\lambda} I(\lambda)}$$

Where L corresponds to the total wavelength range, $I(\lambda)$ the intensity at a given wavelength and given pixel, and n is the harmonic order. Thus, after the transformation the emission spectra is transformed into a phasor, i.e., one single point with coordinates (G, S) and is represented in a polar plot. The angular position of the phasor in the polar plot (the phasor angle) is proportional to the spectral center of mass and the distance from the origin (the phasor radius) is inversely proportional to the width at the half maximum (FWHM). The transformation of the spectral image to phasors results, in the Fourier space (the spectral phasor plot), in a cluster of phasors representing each emission spectrum in the spectral image. The phasor plot has the properties of linear combination and reciprocity. Where the contributions from the different species, and the interactions between them may be analyzed in a straightforward manner as pixels distributes along a line that join the pure components. The reciprocity principle enables us to select regions of interest in the phasor space and color them in the intensity image.

3. Results and discussion

3.1. Framework for the study

The main question to be answered in this work was if changes in the stiffness of the extracellular media would change the membrane structural heterogeneity. To measure membrane heterogeneity, we used the spectral properties of LAURDAN and phasor analysis, a methodology that allows quantification of areas in the membrane having different fluidities.

Several parameters were defined to keep the study within specific boundaries. First, we used NIH-3 T3 mouse fibroblast These cells have

been used before in biophysical studies in traditional cell culture configuration in a culture plate [46] and immersed in collagen type I where they show a distinguished viability [63-67]. Biocompatibility test (Sytox Orange and NucRedLive 647) for NIH 3 T3 cells and collagen, showed a viability percentage of 94.0 \pm 0.5, 94.8 \pm 0.3, 92,5 \pm 2.3 and 91.7 ± 1.8 for the respective collagen concentrations of 0.5, 1.0, 2.0 and 4.0 mg/mL, in agreement with the literature [64,65]. The stiffness range used was based on collagen concentration ranging from 0.5 to 4.0 mg/ mL. Importantly, the preparation was done without modifying the protein or using a cross linker, resulting in relatively low maximum stiffness levels that are typically observed in neurological tissues [68]. The collagen under the experimental conditions formed a gel in 40-45 min. However, to enable the cells to adapt and interact with the collagen, incubation periods of 24 and 72 h were used. Characterization of the collagen matrices were performed without cells, under the assumption that no significant changes will occur to the matrix during the interaction with the cells although it is reported that there is some collagen remodeling induced by NIH-3 T3 cells after 4 days incubation in collagen 2 mg/mL [63].

3.2. Collagen matrix characterization

Collagen matrices of 0.5, 1.0, 2.0 and 4.0 mg/mL were fabricated and incubated for 24 and 72 h at 37 $^{\circ}\text{C}.$

3.2.1. Fiber diameter

Fiber diameters were determined from SEM images. For each collagen concentration 4 images were analyzed. Fig. 1 shows the SEM images for the matrices of different collagen concentrations and the average value for fiber diameter at the two incubation times (24 and 72 h). Collagen matrices at 0.5 mg/mL showed the largest average fiber size, $137 \text{ nm} \pm 23 \text{ nm}$ and $108 \text{ nm} \pm 18 \text{ nm}$ for 24 and 72 h respectively. For the other three collagen concentrations fiber size is in the range of 78 to 90 nm. Observation of the images show that as the collagen concentration increased, the number of fibers and the interfiber interactions

also increased. At 0.5 mg/mL it is possible to observe single fibers but starting from 1.0 mg/mL most of them are associated with others. Single fibers at low collagen concentration are expected to be more hydrated and show a larger diameter that associated fibers. Fiber size depends on the collagen properties (concentration, type and source) and also on incubation time [69–71]; for incubation times over 24 h literature reports fiber sizes around 90 nm [70,71] in agreement with the range obtained from our data.

3.2.2. Fiber occupation volume

The volume occupied by the fibers is inverse to the free volume available for the cells to grow within. To determine the volume occupied by the collagen fibers, second harmonic generation (SHG) signals from collagen were used to acquire FLIM (fluorescence lifetime imaging microcopy) images in several z-planes. As an example of the analysis, Fig. 2A shows the SHG intensity image of one z-plane of a collagen matrix. The FLIM data were Fourier transformed into the phasor representation and plotted in a phasor plot (Fig. 2B). Since the lifetime for SHG signal is zero, all these phasors are located at the beginning of the universal circle [72]. A red circle was used to enclose all the phasor and using the reciprocity principle of the phasor analysis [42], all the phasors inside the cursor were back located in the intensity image (Fig. 2C). From each intensity stack (11 images in z plane) the area occupied by collagen was determined and the volume obtained by the addition of these areas. Fig. 2D show the analysis for one z stack. For each collagen concentration, at the two incubation times, 4 z-stacks were averaged (Fig. 2E). The volume occupied by the fibers increased with the collagen concentration going from 20 to 60 % when comparing 0.5 and 4 mg/mL. As the concentration of collagen increased fibrogenesis is favored by the availability of free collagen chains [71].

3.2.3. Viscoelastic properties

Using oscillatory shear tests, it is possible to study the viscous and elastic properties of the collagen gels. These properties account for the ability of the gel to store (G') or dissipate (G'') energy when the gel is

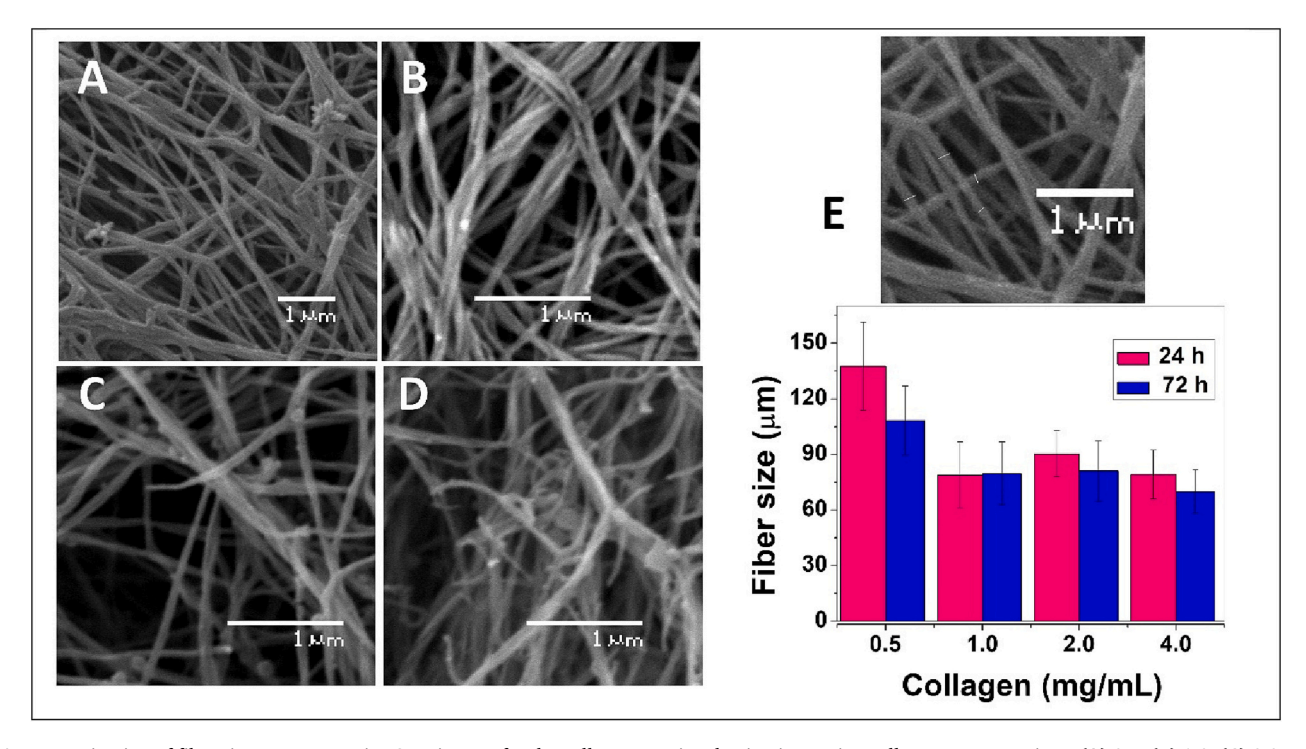


Fig. 1. Determination of fiber size: Representative SEM images for the collagen matrices having increasing collagen concentrations: **(A)** 0.5, **(B)** 1.0, **(C)** 2.0 and **(D)** 4.0 mg/mL. **(E)** Using Image J software, the diameter of 80–90 individual fibers was measured for each collagen concentration and the plot shows fiber diameter as function of the collagen concentration and incubation time. ANOVA test between 24 and 72 h for collagen concentration 0.5 mg/mL showed no significant differences (p > 0.05).

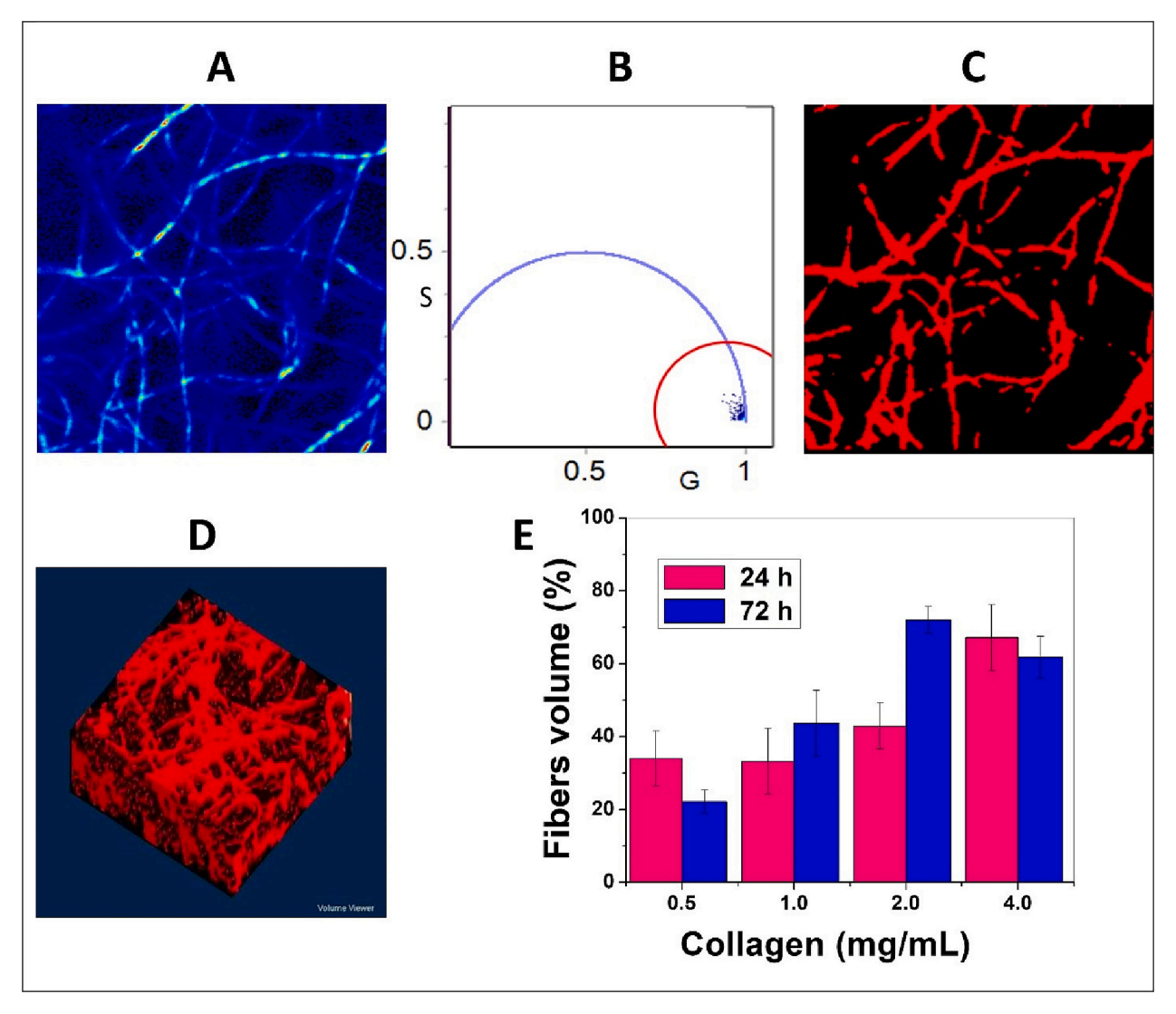


Fig. 2. Volume occupied by collagen fibers. (A) Representative two-dimensional SHG intensity image of a collagen matrix (image size $30 \times 30 \mu m$) (B) FLIM phasor plot showing the phasors (blue dots inside the red circle) at lifetime = zero from the SHG signal. (C) The location of the pixels inside the red circle in B is shown in the intensity image. These pixels are quantified in several images taken in the z axis (D) Tridimensional reconstruction of the pixels occupied by collagen in the matrix. For each collagen matrix concentration, the volume occupied by collagen was measured at 24 (pink) and 72 h (blue). For each condition, 4 different z-stacks were measured, each of them containing 11z-planes, image size $30 \times 30 \times 2 \mu m$. The average occupied volume with the corresponding standard deviation was plotted (E).

subjected to shear stress, providing information about the structural stability of the collagen. The four collagen matrices (concentrations 0.5,1.0, 2.0 and 4 mg/mL) were incubated for 24 and 72 h and Fig. 3 shows the rheological analysis.

Fig. 3A and B show the comparison of the storage (G') and loss (G") modulus as a function of shear strain for the collagen matrices incubated 24 h (Fig. 3A) and 72 h (Fig. 3B). As a general observation, for all collagen concentrations, the G' and G" curves intersected as the applied strain increased. The first intersection was observed at approximately at 0.1–0.25 % oscillation strain, where $G^\prime > G^{\prime\prime}$ indicate the formation of a stiffer structure. This phenomenon is known as strain-stiffening and is associated with both generic contributions of the chains, such as stretching of the biopolymer segments, as well as the formation of more organized structures that decrease energy dissipation [73,74]. Subsequently, for gels of 2.0 and 4.0 mg/mL at deformation close to 25 %, the curves cross again and G'' > G'. This behavior is described in the literature and it is attributed to a strain-softening phenomenon resulting from a redistribution of the internal stress by increasing the sliding of the chain entanglements [75]. Although a higher contribution from G' was expected, Hensen and Mackay explained this behavior using the

unraveling layer model [76]. This model states that at the interface of the instrument geometry and the matrix being measured (geometry/matrix interface), there is a layer of finite thickness with a lower viscosity than the sample, where a more disentangled fiber structure is present [76]. In our case, at the geometry/collagen matrix interface there is an aqueous layer, like the "disentangled layer" proposed by Henson and Mackay, that contributes to the fluidity of the sample and is responsible for the increased G" values. Furthermore, the contribution of this layer is observed to be more prominent at low collagen concentrations, where more solvent is present in the matrix.

Focusing on the changes of G' value, storage modulus (open circles in Fig. 3A and B), as a function of shear stress for the collagen matrices at the two gelation times some interesting changes may be mentioned. The observed overall decrease in G' modulus with deformation observed for all the collagen concentration and at the two incubation times may be attributed to the absence of chemical crosslinking (covalent bonds) in the matrices. Thus, the structural stability of the gel is given by intermolecular forces that are more sensitive to mechanical stress and lead to a material with lower stiffness. A linear viscoelastic region observed between 0.1 and 10 % deformation is attributed to fiber orientation and

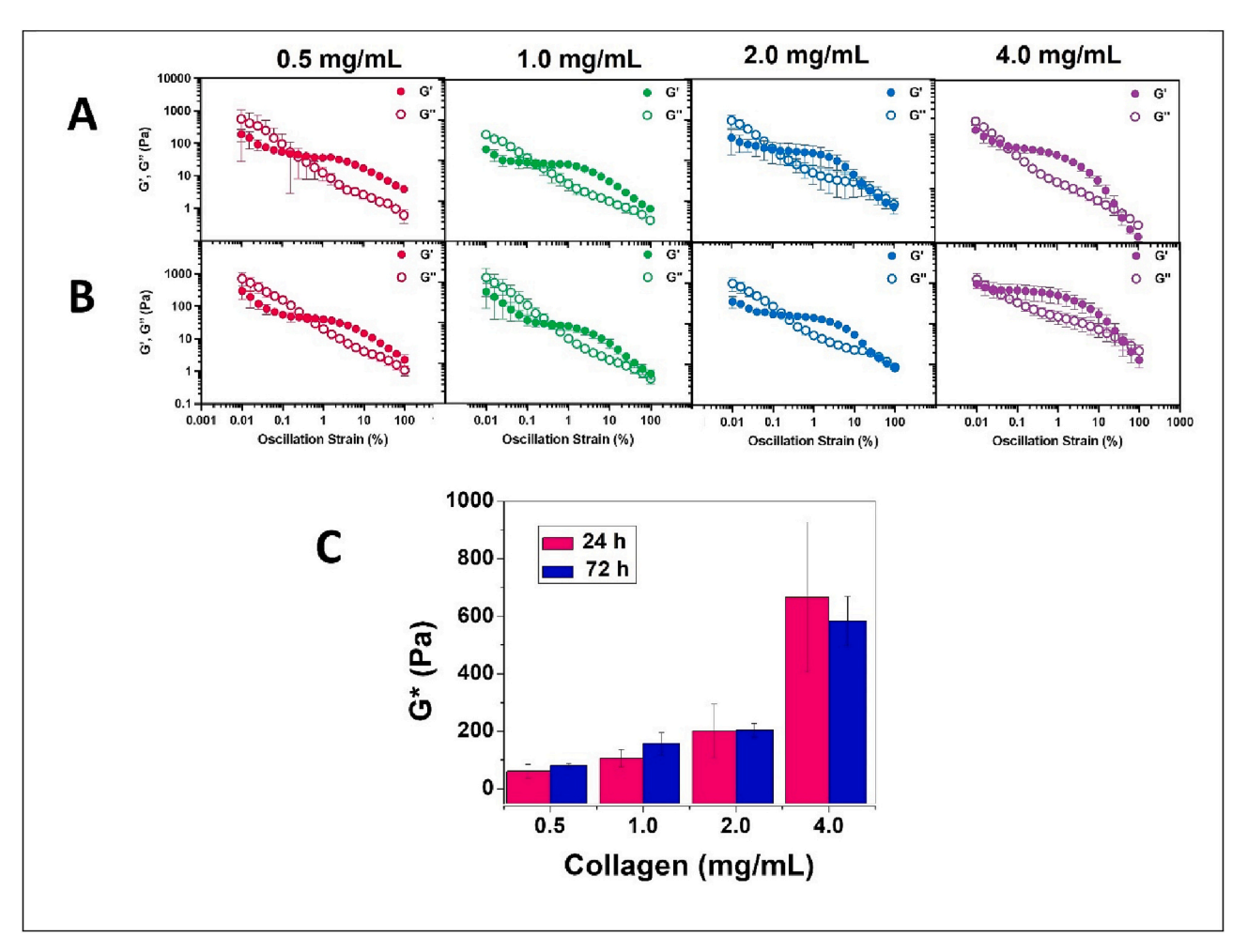


Fig. 3. Viscoelastic properties of collagen matrices. Oscillatory amplitude shear test for collagen gels obtained at gelation time of **(A)** 24 h and **(B)** 72 h. **(C)** Complex module (G^*) versus collagen concentration determined at 0,25 % shear deformation. Store modulus (G'), closed circles), loss modulus (G''), opened circles). ANOVA test between 24 and 72 h for each collagen concentration showed no significant differences (p > 0.05).

alignment [77]. In this linear region, for the two gelation times, the G' value increases with collagen concentration, i.e. an increase in stiffness is observed as collagen concentration increases. This expected behavior can be explained since high concentrations of collagen accelerate fibrogenesis by increasing the availability of free collagen chains [71]. The G' values obtained (100 Pa and 1000 Pa for 0.5 mg/mL and 4 mg/mL, respectively) are higher than the values reported in the literature [73,75,78]. However, this difference may be attributed to the longer gelation time used (24–72 h); in fact, literature reports indicate that there is a progressive increase in the value of modulus, as the gelation time of the collagen increases [79,80]. Under this scenario, the modulus G' values obtained in this work agree with the values obtained for gels formed with similar gelation times [71].

To compare the stiffness of the collagen matrices, the complex module G* (complex modulus) was determined at the linear viscoelastic region (Fig. 3C), more specifically at shear deformation of 0.25 %. In this plot the correlation between collagen concentration and stiffness of the matrices can be clearly observed [75,78]. A small increase in stiffness may be observed when comparing 24 and 72 h gelation time, however ANOVA test for the G* values show this difference to be insignificant (p > 0.05).

3.3. Membrane heterogeneity and the influence of collagen stiffness

Membrane heterogeneity was studied using the fluorescent dye LAURDAN and 3D hyperspectral images of cells were analyses by phasor

plot analysis. To better understand the results it is important to clarify what the techniques measures. In simple terms, LAURDAN senses membrane polarity, P, (related to the number of water molecules present in the bilayer) and dipolar relaxation, DR, (related to reorientation of the water dipoles by rotation, in response to the change in LAURDAN's dipole moment upon excitation). These two terms depend on the lipid order. The term "fluidity" is a qualitative general term used to describe membrane viscosity (capability of the lipids to flow or rotate), and is determined by the water content, the water relaxation, and the lipid order of the bilayer. In the LAURDAN spectral phasor analysis, the information obtained on polarity and DR is mixed and therefore the information obtained from this type of analysis is related to the general term "fluidity".

NIH-3 T3 cells grown inside collagen matrices having different collagen concentrations (Fig. 4A) were compared with control cells grown in a traditional cell culture configuration in a monolayer (Fig. 4B). Hyperspectral images in several z positions (Fig. 4C) were transformed into spectral phasors plots (Fig. 4D). The spectral phasor plot shows a cluster organized along a line indicating shifted LAURDAN spectra sensing environments with different fluidities in the membrane. The two extremes correspond to pixels where LAURDAN is in a fluid (left) or ordered (right) environment. Spectral phasor points along the line correspond to pixels with different fraction of order and fluid components

To analyze the cluster, regions in the membrane with different fluidities are identified using the cursor selection tool. Analysis may

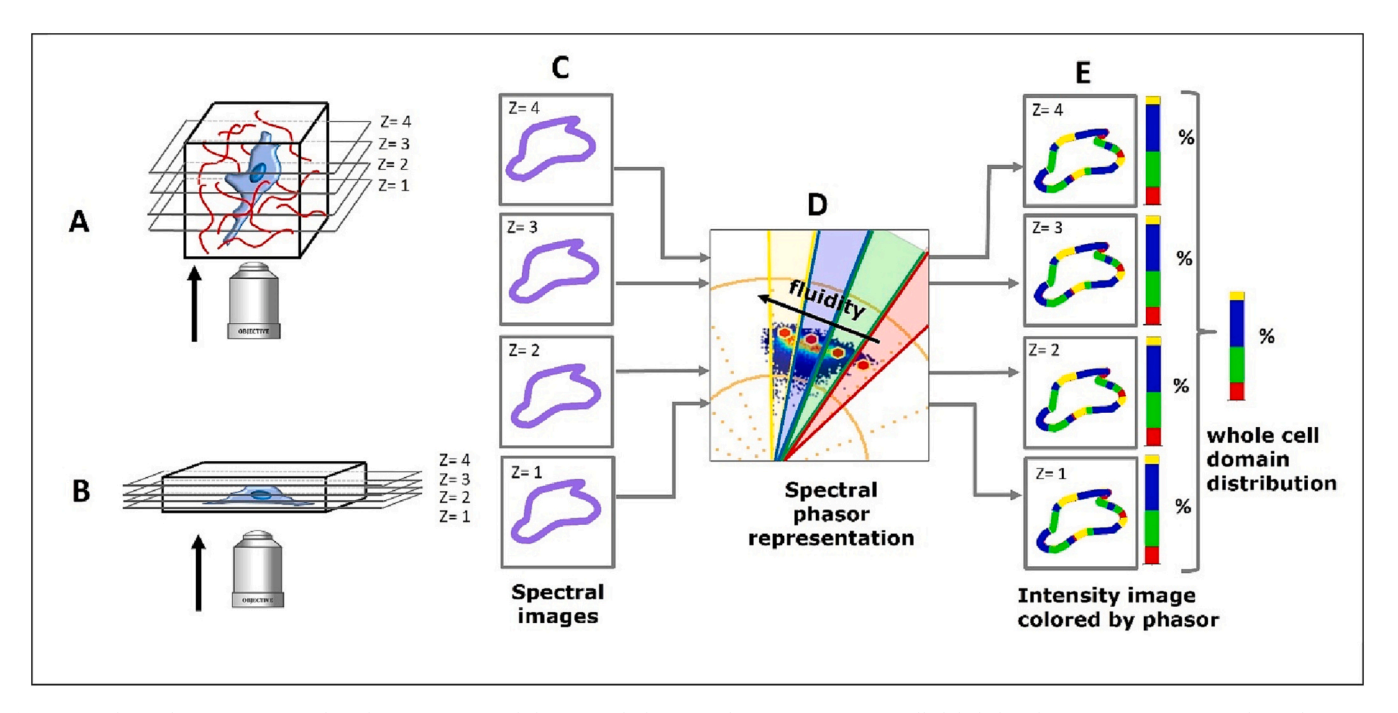


Fig. 4. Membrane heterogeneity analysis by LAURDAN and the spectral phasor analysis: (A) NIH-3 T3 cells labeled with LAURDAN were growth inside matrices having different collagen concentrations, (B) as a control, cells were growth in culture plates as a monolayer. Hyperspectral images were taken in different z planes. (C) For the analysis, the pixels in the images corresponding to the border of the cells (pixels containing the plasma membrane) were isolated, therefore there is no contribution from the other membranous component on the cells (D) The images were transformed into phasors and plotted in a spectral phasor plot. Four angular cursors were used for the analysis (red, green, blue, and yellow). (E) Pixels in the Intensity images were colored according to the location of the cursors and the percentage of each color is represented in a columnar plot. The whole cell heterogeneity distribution was calculated by averaging the different areas analyzed in all the z planes. SimFCS software was used for this analysis.

consider two extreme cursors linked [52] or a discrete number of nonlinked cursors [41] depending on the application. In this work, four angular cursors (shown as triangles in Fig. 4D) were used to define four areas in the membrane with different fluidities: red and yellow angular cursors indicate ordered or fluid areas, respectively, while blue and green angular cursors represent areas with intermediate fluidities as

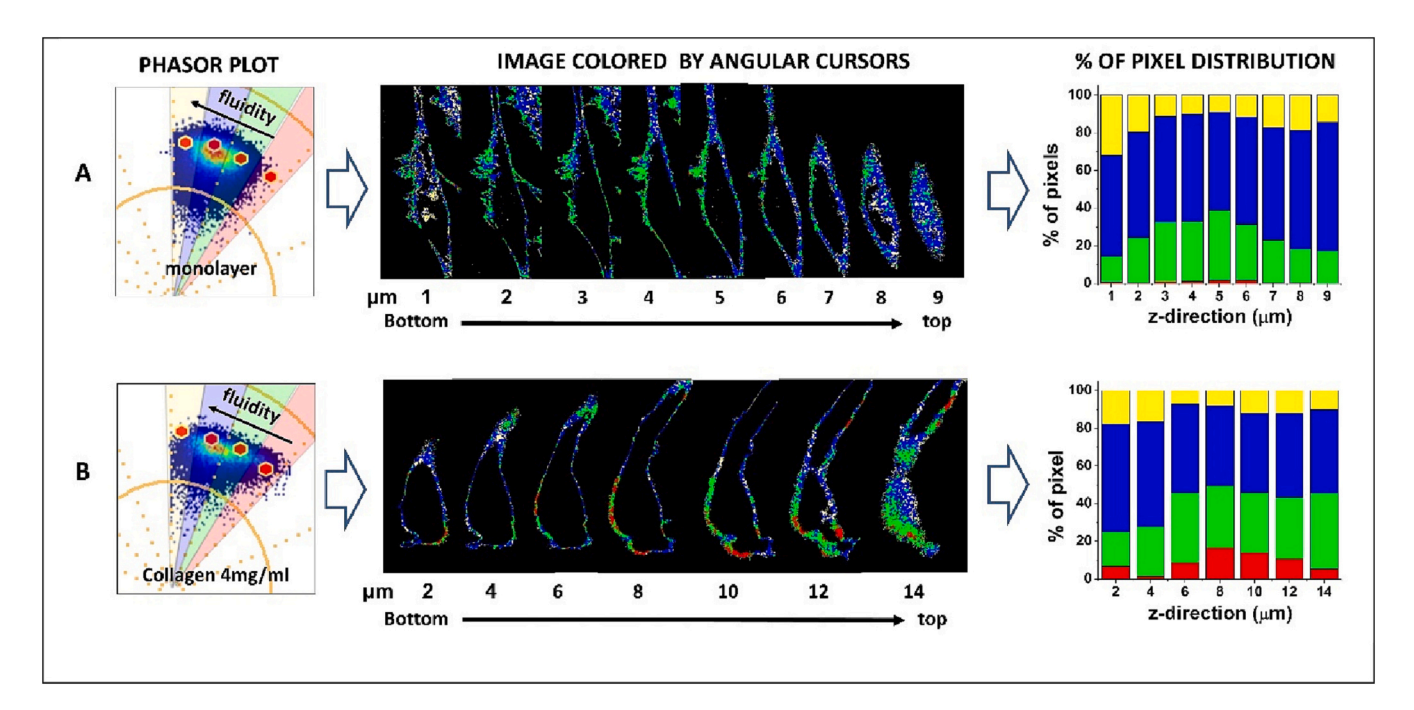


Fig. 5. Membrane heterogeneity of NIH-3 T3 grown in a monolayer versus in a 3D culture inside collagen matrix using LAURDAN: Representative spectral phasor analysis of NIH-3 T3 cells stained with LAURDAN and cultured in: (A) a monolayer (typical configuration) or (B) inside 4 mg/mL collagen for 24 h at 37 $^{\circ}$ C. The phasor plot shows a cluster of phasors from 9 hyperspectral images taken every 1 μ m along the z axis from bottom to top of the cell. Four angular cursors were used for the analysis indicating from order (red) to more fluid (yellow) areas. Pixels located inside each cursor are located back on the intensity image with the respective color generating an image colored by angular phasors. The percentage of each colored pixel in the whole cell is plotted in a pixel distribution plot.

linear combination of the ordered and fluid environments. Using the reciprocity principle [42,44,46] of phasor analysis, the phasor points inside each cursor were back located in the intensity image creating a phasor-colored image (Fig. 4E) where the location of the signal can be identified. Fig. 4E also show column plots with the percentages of pixels of each color, representing the distribution of the four referential areas in the membrane [20,41,42]. We used this column plot to study the fluidity distribution under different configurations. The changes in the number and spatial distribution of the pixels indicate changes in the membrane fluidity distribution generated by the applied stimulus.

Fig. 5 shows the analysis of a representative z-stack for the two extreme cases studied, cells grown in a monolayer (Fig. 5A) and 3D cell culture inside a 4 mg/mL collagen matrix (Fig. 5B) after 72 h. Visual comparison of the two spectral phasor plots and using the four angular cursors (red, green, blue and yellow) shows a population of phasors (colored in red) which is only present in the cells grown immersed in collagen and not in cells in monolayer. This population corresponds to more ordered areas in the membrane and their location is shown for the two cases in the intensity image colored according to the angular cursors (Fig. 5A and B). The percentage of pixel distribution analysis (Fig. 5A and B) shows a different distribution of fluidity domains in both situations. After analyzing independently 16 cells and not finding a clear correlation between the z-position and the percentage of pixel distribution we decided to use the average distribution of all the z-positions for further analysis. Overall, membranes of cells cultured as monolayers are more fluid than cells in contact with collagen fibers at 4 mg/mL. An additional observation from the z section examined to image the full cells is that cells in the monolayer (9 μ m) were almost half the size of the ones in collagen (14 µm) (Fig. 5A and B), indicating that cells immersed in collagen (4 mg/mL after 72 h) acquired a 3D position inside the collagen.

Fig. 6 show the analysis performed for cells grown inside collagen matrices of different concentrations and at the two incubation times studied, i.e., 24 h and 72 h. After 24 h incubation, the pixel distribution analysis (Fig. 6A) shows pixels with different fractions of ordered and fluid components, mostly the ones represented by yellow, blue, and green cursors but with a small presence of the most ordered domains (red). After 72 h, the presence of the more rigid domains is established, and their percentage increased with collagen concentration. The size of the cells in the z-direction (Fig. 6B), indicative of cells adopting a 3D configuration, also changed as collagen concentration increased both at 24 h and 72 h. At 0.5 mg/mL and 24 h, the cells already adopted a 3D configuration inside the collagen fibers. The dispersion of the data at 24 h (standard deviation) as compared with 72 h show the stabilization of the cells inside the matrix with incubation time.

4. Conclusions

In our experimental setup, cells were incubated with increasing concentrations of collagen to allow the formation of collagen fibers around them. As collagen concentration and gelation time increased it is expected that, as cells experience the reduction of the free space, the stiffness of the matrix increases, and consequently, the compression forces the cells experience, and the collagen-cells contacts increase. Our data show all these changes.

(a) After 24 h, the distribution of membrane fluidity domains is similar and independent of the collagen concentration. At this time cells in collagen are in a 3D configuration inside the collagen and the fluidity does not differ significantly from the cells in the dish configuration, even if the last ones are flat and attached to the plate.

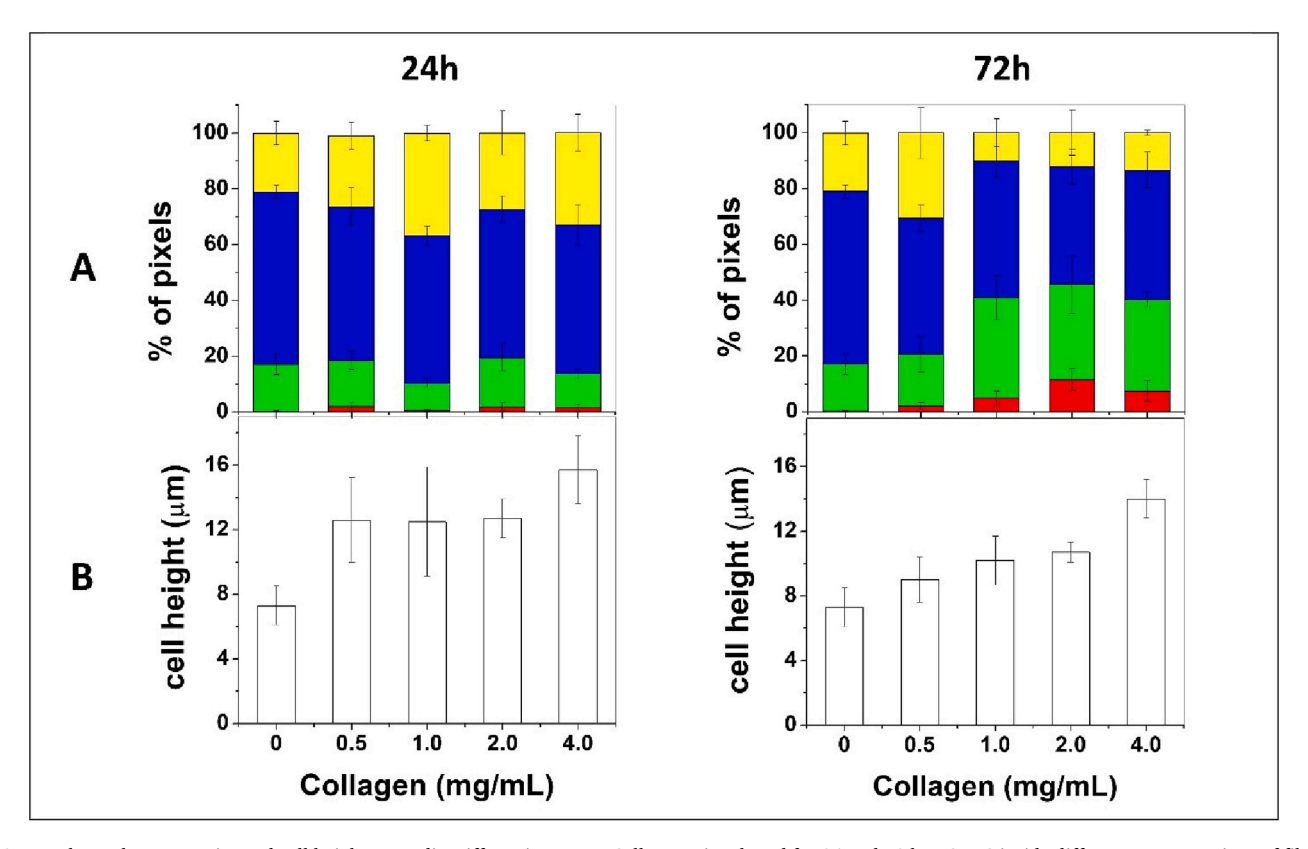


Fig. 6. Membrane heterogeneity and cell height as media stiffness increases: Cells were incubated for 24 and 72 h at 37 $^{\circ}$ C inside different concentrations of fibrillar collagen. **(A)** Percentage of pixel distribution and **(B)** height in micrometers for cells grown inside collagen matrices at different collagen concentrations. Spectral analyses were performed on 50–70 images for each collagen concentration and standard deviations for the analysis are shown. ANOVA tests for ordered domains (red) showed significant differences (p > 0.05) between each collagen concentration and the control without collagen.

(b) After 72 h, collagen properties do not change significantly (fiber size, fiber volume, stiffness) with respect to the 24 h incubation, but the distribution of the membrane fluidity changed. The percentage of ordered regions in the membrane increased as collagen increased, and a new population of more ordered regions appeared.

It is well reported that ECM stiffness can influence cell function [9-16], however, the details of the mechanisms involved are not well established. Experimental results support the direct interaction of membrane receptors with ECM components and that changes in the lipid domains distribution are responsible for triggering the receptors [34-36]. Yamamoto et al., using LAURDAN and the Generalized Polarization technique, reported changes in membrane general fluidity, lipid order and cholesterol content as a response to mechanical stimulus shear stress [37]. They propose that membrane physical properties are involved in the mechano-transduction activating membrane receptors specific to each force [37]. Our data using LAURDAN and spectral phasor analysis show that upon increasing collagen concentration and the stiffness of the media, a redistribution of membrane fluidity regions occurs, specifically, an increase in highly ordered areas and a decrease in the more fluid ones. Our data does not respond to the logical question if these changes in the distribution are induced by the forces created around the cells by the increasing stiffness or by the direct interaction of collagen with specific receptors at the membrane. Our experimental setup did not correlate these events spatially or temporally.

CRediT authorship contribution statement

Joao Aguilar: Software, Formal analysis, Investigation, Data Curation. Leonel Malacrida: Validation, Software Investigation, Writing – review and editing. German Gunther: Methodology Writing – review and editing Visualization. Belén Torrado: Investigation (data collection), Writing – review and editing. Viviana Torres: Writing–review and editing, Visualization. Bruno F. Urbano: Conceptualization, Methodology, Validation, Formal analysis, Resources, Data Curation, Writing-original draft. Susana A. Sánchez: Conceptualization, Methodology, Validation, Formal analysis, Investigation (data collection), Investigation (data collection), Resources, Data Curation, Writing-original draft, Visualization, Supervision, Project administration, Funding Acquisition.

Declaration of competing interest

The authors declare that they have no known competing financial interests or personal relationships that could have appeared to influence the work reported in this paper.

Data availability

The data generated during the current study are available from the corresponding author on reasonable request.

Acknowledgments

German Gunther is supported by Agencia Nacional de Investigación y Desarrollo (ANID), Fondecyt 1160705 and 1200597. Leonel Malacrida is supported by FOCEM (Fondo para la Convergencia Estructural del Mercosur, COF 03/11) and as Imaging Scientist by grant number 2020-225439 from the Chan-Zuckerberg Initiative DAF, an advised fund of Silicon Valley Community Foundation. Bruno F. Urbano is supported by ANID, Fondecyt 1171082 and 1211450. Susana A. Sánchez is supported by ANID, Fondecyt 1201028.

References

- [1] K. Fredriksson, X.D. Liu, J. Lundahl, J. Klominek, S.I. Rennard, C.M. Skold, Red blood cells increase secretion of matrix metalloproteinases from human lung fibroblasts in vitro, Am. J. Phys. Lung Cell. 290 (2006) L326–L333.
- [2] P. Boutouyrie, A.I. Tropeano, R. Asmar, I. Gautier, A. Benetos, P. Lacolley, S. Laurent, Aortic stiffness is an independent predictor of primary coronary events in hypertensive patients - a longitudinal study, Hypertension 39 (2002) 10–15.
- [3] S.L. Schnider, R.R. Kohn, Glucosylation of human collagen in aging and diabetes mellitus, J. Clin. Invest. 66 (1980) 1179–1181.
- [4] R.G. Harrison, Observations on the living developing nerve fiber, Anat. Rec. 1 (1907) 116–118.
- [5] J.R.W. Conway, C. Vennin, A.S. Cazet, D. Herrmann, K.J. Murphy, S.C. Warren, L. Wullkopf, A. Boulghourjian, A. Zaratzian, A.M. Da Silva, M. Pajic, J.P. Morton, T. R. Cox, P. Timpson, Three dimensional organotypic matrices from alternative collagen sources as pre-clinical models for cell biology, Sci. Rep. 7 (2017) 1–15.
- [6] M. Kato, R. Hayashi, Effects of high pressure on lipids and biomembranes for understanding high-pressure-induced biological phenomena, Biosci. Biotechnol. Biochem. 63 (1999) 1321–1328.
- [7] A.N. Gasparski, K.A. Beningo, Mechanoreception at the cell membrane: more than the integrins, Arch. Biochem. Biophys. 586 (2015) 20–26.
- [8] D. Mitrossilis, J. Fouchard, D. Pereira, F. Postic, A. Richert, M. Saint-Jean, A. Asnacios, Real-time single-cell response to stiffness, Proc. Natl. Acad. Sci. U. S. A. 107 (2010) 16518–16523.
- [9] A.M. Handorf, Y.X. Zhou, M.A. Halanski, W.J. Li, Tissue stiffness dictates development, homeostasis, and disease progression, Organogenesis 11 (2015) 1–15
- [10] F.M. Watt, W.T.S. Huck, Role of the extracellular matrix in regulating stem cell fate, Nat. Rev. Mol. Cell Biol. 14 (2013) 467–473.
- [11] H.W. Lv, L.S. Li, M.Y. Sun, Y. Zhang, L. Chen, Y. Rong, Y.L. Li, Mechanism of regulation of stem cell differentiation by matrix stiffness, Stem Cell Res Ther 6 (2015) 103.
- [12] C.M. Lo, H.B. Wang, M. Dembo, Y.L. Wang, Cell movement is guided by the rigidity of the substrate, Biophys. J. 79 (2000) 144–152.
- [13] P. Muller, U. Bulnheim, A. Diener, F. Luthen, M. Teller, E.D. Klinkenberg, H. G. Neumann, B. Nebe, A. Liebold, G. Steinhoff, J. Rychly, Calcium phosphate surfaces promote osteogenic differentiation of mesenchymal stem cells, J. Cell. Mol. Med. 12 (2008) 281–291.
- [14] J. Solon, I. Levental, K. Sengupta, P.C. Georges, P.A. Janmey, Fibroblast adaptation and stiffness matching to soft elastic substrates, Biophys. J. 93 (2007) 4453–4461.
- [15] A. Saez, M. Ghibaudo, A. Buguin, P. Silberzan, B. Ladoux, Rigidity-driven growth and migration of epithelial cells on microstructured anisotropic substrates, Proc. Natl. Acad. Sci. U. S. A. 104 (2007) 8281–8286.
- [16] D. Mitrossilis, J. Fouchard, A. Guiroy, N. Desprat, N. Rodriguez, B. Fabry, A. Asnacios, Single-cell response to stiffness exhibits muscle-like behavior, Proc. Natl. Acad. Sci. U. S. A. 106 (2009) 18243–18248.
- [17] D.A. Brown, E. London, Structure and function of sphingolipid and cholesterol rich membrane rafts, J. Biol. Chem. 275 (2000) 17221–17224.
- [18] C. Gomez-Mouton, J.L. Abad, E. Mira, R.A. Lacalle, E. Gallardo, S. Jimenez-Baranda, I. Illa, A. Bernad, S. Manes, C. Martinez-A, Segregation of leading-edge and uropod components into specific lipid rafts during T cell polarization, Proc. Natl. Acad. Sci. U. S. A. 98 (2001) 9642–9647.
- [19] K. Jacobson, O.G. Mouritsen, R.G.W. Anderson, Lipid rafts: at a crossroad between cell biology and physics, Nat. Cell Biol. 9 (2007) 7–14.
- [20] S.A. Sanchez, M.A. Tricerri, E. Gratton, Laurdan generalized polarization fluctuations measures membrane packing micro-heterogeneity in vivo, Proc. Natl. Acad. Sci. U. S. A. 109 (2012) 7314–7319.
- [21] K. Simons, R. Ehehalt, Cholesterol, lipid rafts, and disease, J. Clin. Invest. 110 (2002) 597–603.
- [22] K. Simons, D. Toomre, Lipid rafts and signal transduction, Nat. Rev. Mol. Cell Biol. 1 (2000) 31–39.
- [23] L.D. Zajchowski, S.M. Robbins, Lipid rafts and little caves compartmentalized signalling in membrane microdomains, Eur. J. Biochem. 269 (2002) 737–752.
- [24] M. Tanaka, T. Kikuchi, H. Uno, K. Okita, T. Kitanishi-Yumura, S. Yumura, Turnover and flow of the cell membrane for cell migration, Sci. Rep. 7 (2017) 12970.
- [25] P. Noutsi, E. Gratton, S. Chaieb, Assessment of membrane fluidity fluctuations during cellular development reveals time and cell type specificity, PLoS One 30 (2016), e0158313.
- [26] S. Manes, R. Ana Lacalle, C. Gomez-Mouton, A.C. Martinez, From rafts to crafts: membrane asymmetry in moving cells, Trends Immunol. 24 (2003) 320–326.
- [27] T.D. Ross, B.G. Coon, S. Yun, N. Baeyens, K. Tanaka, M. Ouyang, M.A. Schwartz, Integrins in mechanotransduction, Curr. Opin. Cell Biol. 25 (2013) 613–618.
- [28] Y. Wang, B.S. Maciejewski, D. Drouillard, M. Santos, M.A. Hokenson, R.L. Hawwa, Z. Huang, J. Sanchez-Esteban, A role for caveolin-1 in mechanotransduction of fetal type II epithelial cells, Am. J. Phys. Lung Cell. Mol. Phys. 298 (2010) 1775–1783
- [29] M. Isshiki, J. Ando, K. Yamamoto, T. Fujita, Y. Ying, R.G.W. Anderson, Sites of Ca2 + wave initiation move with caveolae to the trailing edge of migrating cells, J. Cell Sci. 115 (2002) 475–484.
- [30] J. Yu, S. Bergaya, T. Murata, I.F. Alp, M.P. Bauer, M.I. Lin, M. Drab, T. V. Kurzchalia, R.V. Stan, W.C. Sessa, Direct evidence for the role of caveolin-1 and caveolae in mechanotransduction and remodeling of blood vessels, J. Clin. Invest. 116 (2006) 1284–1291.
- [31] Y.C. Yeh, J.Y. Ling, W.C. Chen, H.H. Lin, M.J. Tang, Mechanotransduction of matrix stiffness in regulation of focal adhesion size and number: reciprocal regulation of caveolin-1 and beta1 integrin, Sci. Rep. 7 (2017) 15008.

- [32] B. Roy, D. Carugo, X. Zhang, T.K. Maiti, S. Chakraborty, The role of membrane lipid rafts in osteoblastic sensing and propagation of mechanical forces: a microfluidic based single cell analysis study, in: 16th International Conference on Miniaturized Systems for Chemistry and Life Sciences October 28 - November 1, Okinawa, Japan, 2012.
- [33] E.N. Petersen, H.-W. Chung, A. Nayebosadri, S.B. Hansen, Kinetic disruption of lipid rafts is a mechanosensor for phospholipase D, Nat. Commun. 7 (2016) 13873.
- [34] M. Zhao, J. Pu, J.V. Forrester, C.D. McCaig, Membrane lipids, EGF receptors, and intracellular signals colocalize and are polarized in epithelial cells moving directionally in a physiological electric field, FASEB J. 16 (2002) 857–859.
- [35] B.J. Lin, S.H. Tsao, A. Chen, S.K. Hu, L. Chao, P.G. Chao, Lipid rafts sense and direct electric field-induced migration, Proc. Natl. Acad. Sci. U. S. A. 114 (2017) 8568–8573.
- [36] B. Sinha, D. Koster, R. Ruez, P. Gonnord, M. Bastiani, D. Abankwa, R.V. Stan, G. Butler-Browne, B. Vedie, L. Johannes, N. Morone, R.G. Parton, G. Raposo, P. Sens, C. Lamaze, P. Nassoy, Cells respond to mechanical stress by rapid disassembly of caveolae, Cell 144 (2011) 402–413.
- [37] K. Yamamoto, Y. Nogimori, H. Imamura, J. Ando, Shear stress activates mitochondrial oxidative phosphorylation by reducing plasma membrane cholesterol in vascular endothelial cells, Proc. Natl. Acad. Sci. U. S. A. 117 (2020) 33660–33667
- [38] K. Yamamoto, J. Ando, Vascular endothelial cell membranes differentiate between stretch and shear stress through transitions in their lipid phases, Am. J. Physiol. Heart Circ. Physiol. 309 (2015) H1178–H1185.
- [39] K. Yamamoto, J. Ando, Emerging role of plasma membranes in vascular endothelial mechanosensing, Circ. J. 82 (2018) 2691–2698.
- [40] T. Parasassi, E.K. Krasnowska, L. Bagatolli, A.E. Gratton, Laurdan and Prodan as polarity-sensitive fluorescent membrane probes, J. Fluoresc. 8 (1998) 365–373.
- [41] G. Günther, V. Herlax, M.P. Lillo, C. Sandoval-Altamirano, L.N. Belmar, S. A. Sánchez, Study of rabbit erythrocytes membrane solubilization by sucrose monomyristate using laurdan and phasor analysis, Colloids Surf. B: Biointerfaces 161 (2018) 375–385.
- [42] G. Gunther, L. Malacrida, D.M. Jameson, E. Gratton, S.A. Sanchez, LAURDAN since weber: the quest for visualizing membrane heterogeneity, Acc. Chem. Res. 54 (2021) 976–987.
- [43] O. Golfetto, E. Hinde, E. Gratton, The Laurdan spectral phasor method to explore membrane micro-heterogeneity and lipid domains in live cells, Methods Mol. Biol. 1232 (2015) 273–290.
- [44] L. Malacrida, E. Gratton, D.M. Jameson, Model-free methods to study membrane environmental probes: a comparison of the spectral phasor and generalized polarization approaches, Methods Appl. Fluoresc. 3 (2015), 019601.
- [45] T. Parasassi, G. Ravagnan, R.M. Rusch, E. Gratton, Modulation and dynamics of phase properties in phospholipid mixtures detected by Laurdan fluorescence, Photochem. Photobiol. 57 (1993) 403–410.
- [46] L. Malacrida, D.M. Jameson, E. Gratton, A multidimensional phasor approach reveals LAURDAN photophysics in NIH-3T3 cell membranes, Sci. Rep. 7 (2017) 9215.
- [47] T. Parasassi, G. De Stasio, G. Ravagnan, R.M. Rusch, E. Gratton, Quantitation of lipid phases in phospholipid vesicles by the generalized polarization of LAURDAN fluorescence, Biophys. J. 60 (1991) 179–189.
- [48] T. Parasassi, E. Gratton, W.M. Yu, P. Wilson, M. Levi, Two-photon fluorescence microscopy of laurdan generalized polarization domains in model and natural membranes, Biophys. J. 72 (1997) 2413–2429.
- [49] T. Parasassi, M. Di Stefano, M. Loiero, G. Ravagnan, E. Gratton, Influence of cholesterol on phospholipid bilayers phase domains as detected by Laurdan fluorescence, Biophys. J. 66 (1994) 120–132.
- [50] T. Parasassi, E. Gratton, Membrane lipid domains and dynamics as detected by Laurdan fluorescence, J. Fluoresc. 5 (1995) 59–69.
- [51] L. Malacrida, E. Gratton, LAURDAN fluorescence and phasor plots reveal the effects of a H2O2 bolus in NIH-3T3 fibroblast membranes dynamics and hydration, Free Radic. Biol. Med. (2018) 144–156.
- [52] S. Sameni, L. Malacrida, Z. Tan, M.A. Digman, Alteration in fluidity of cell plasma membrane in Huntington disease revealed by spectral phasor analysis, Sci. Rep. 8 (2018) 734.
- [53] D. Rodriguez-Agudo, L. Malacrida, G. Kakiyama, T. Sparrer, C. Fortes, M. Maceyka, M.A. Subler, J.J. Windle, E. Gratton, W.M. Pandak, G. Gil, StarD5: an ER stress protein regulates plasma membrane and intracellular cholesterol homeostasis, J. Lipid Res. 60 (2019) 1087–1098.
- [54] F. Sena, M. Sotelo-Silveira, S. Astrada, M.A. Botella, L. Malacrida, O. Borsani, Spectral phasor analysis reveals altered membrane order and function of root hair cells in Arabidopsis dry2/sqe1-5 drought hypersensitive mutant, Plant Physiol. Biochem. 119 (2017) 224–231.

- [55] J.L. Bron, G.H. Koenderink, V. Everts, T.H. Smit, Rheological characterization of the nucleus pulposus and dense collagen scaffolds intended for functional replacement, J. Orthop. Res. 27 (2009) 620–626.
- [56] T.C. Baradet, J.C. Haselgrove, J.W. Weisel, Three dimensional reconstruction of fibrin clot networks from stereoscopic intermediate voltage electron microscope images and analysis of branching, Biophys. J. 68 (1995) 1551–1560.
- [57] A. Dvornikov, L. Malacrida, E. Gratton, The DIVER microscope for imaging in scattering media, Methods Protoc. 2 (2019) 53.
- [58] M.A. Digman, V.R. Caiolfa, M. Zamai, E. Gratton, The phasor approach to fluorescence lifetime imaging analysis, Biophys. J. 94 (2008) L14–L16.
- [59] D.M. Jameson, E. Gratton, R. Hall, The measurement and analysis of heterogeneous emissions by multifrequency phase and modulation fluorometry, Appl. Spectrosc. Rev. 20 (1984) 55–106.
- [60] G. Redford, R. Clegg, Polar plot representation for frequency-domain analysis of fluorescence lifetimes, J. Fluoresc. 15 (2005) 805–815.
- [61] N.G. James, J.A. Ross, M. Stefl, D.M. Jameson, Applications of phasor plots to in vitro protein studies, Anal. Biochem. 410 (2011) 70–76.
- [62] F. Fereidouni, A.N. Bader, H.C. Gerritsen, Spectral phasor analysis allows rapid and reliable unmixing of fluorescence microscopy spectral images, Opt. Express 20 (2012) 12729–12741.
- [63] C.-L. Chiu, M.A. Digman, E. Gratton, Cell matrix remodeling ability shown by image spatial correlation, J. Biophys. 2013 (2013) 1–8.
- [64] E.O. Osidak, P.A. Karalkin, M.S. Osidak, V.A. Parfenov, D.E. Sivogrivov, F. Pereira, A.A. Gryadunova, E.V. Koudan, Y.D. Khesuani, C.V.A. Capital Ka, S.I. Belousov, S. V. Krasheninnikov, T.E. Grigoriev, S.N. Chvalun, E.A. Bulanova, V.A. Mironov, S. P. Domogatsky, Viscoll collagen solution as a novel bioink for direct 3D bioprinting, J. Mater. Sci. Mater. Med. 30 (2019) 31.
- [65] S. Riedel, P. Hietschold, C. Krömmelbein, T. Kunschmann, R. Konieczny, W. Knolle, Claudia T. Mierke, M. Zink, M.S. G., Design of biomimetic collagen matrices by reagent-free electron beam induced crosslinking: structure-property relationships and cellular response, Mater. Des. 168 (2019), 107606.
- [66] Y. Wang, W. Zhang, J. Yuan, J. Shen, Differences in cytocompatibility between collagen, gelatin and keratin, Mater. Sci. Eng. C Mater. Biol. Appl. 59 (2016) 30–34
- [67] E. Turker, U.H. Yildiz, A. Yildiz, Biomimetic hybrid scaffold consisting of coelectrospun collagen and PLLCL for 3D cell culture, Int. J. Biol. Macromol. 139 (2019) 1054–1062.
- [68] A.J. Engler, S. Sen, H.L. Sweeney, D.E. Discher, Matrix elasticity directs stem cell lineage specification, Cell 126 (2006) 677–689.
- [69] S.T. Kreger, B.J. Bell, J. Bailey, E. Stites, J. Kuske, B. Waisner, S.L. Voytik-Harbin, Polymerization and matrix physical properties as important design considerations for soluble collagen formulations, Biopolymers 93 (2010) 690–707.
- [70] C.B. Raub, V. Suresh, T. Krasieva, J. Lyubovitsky, J.D. Mih, A.J. Putnam, B. J. Tromberg, S.C. George, Noninvasive assessment of collagen gel microstructure and mechanics using multiphoton microscopy, Biophys. J. 92 (2007) 2212–2222.
- [71] B.J.W. Zhang, L. He, C. Xu, D. Xie, K.-W. Paik, H. Wang, Systematic modulation of gelation dynamics of snakehead (Channa argus) skin collagen by environmental parameters, Macromol. Res. 25 (2017) 1105–1114.
- [72] S. Ranjit, A. Dvornikov, M. Levi, S. Furgeson, E. Gratton, Characterizing fibrosis in UUO mice model using multiparametric analysis of phasor distribution from FLIM images, Biomed. Opt. Express 7 (2016) 3519–3530.
- [73] S. Motte, L.J. Kaufman, Strain stiffening in collagen I networks, Biopolymers 99 (2013) 35–46.
- [74] C. Storm, J.J. Pastore, F.C. MacKintosh, T.C. Lubensky, P.A. Janmey, Nonlinear elasticity in biological gels, Nature 435 (2005) 191–194.
- [75] N.A. Kurniawan, L.H. Wong, R. Rajagopalan, Early stiffening and softening of collagen: interplay of deformation mechanisms in biopolymer networks, Biomacromolecules 13 (2012) 691–698.
- [76] D.J. Henson, Effect of gap on the viscosity of monodisperse polystyrene melts: slip effects, J. Rheol. 39 (1995) 359.
- [77] F. Burla, S. Dussi, C. Martinez-Torres, J. Tauber, J. van der Gucht, H. Koenderink Gijsje, Connectivity and plasticity determine collagen network fracture, Proc. Natl. Acad. Sci. U. S. A. 117 (2020) 8326–8334.
- [78] D. Vader, A. Kabla, D. Weitz, L. Mahadevan, Strain-induced alignment in collagen gels, PLoS One 4 (2009), e5902.
- [79] B.A. Roeder, K. Kokini, J.E. Sturgis, J.P. Robinson, S.L. Voytik-Harbin, Tensile mechanical properties of three-dimensional type I collagen extracellular matrices with varied microstructure, J. Biomech. Eng. 124 (2002) 214–222.
- [80] K. Madhavan, D. Belchenko, A. Motta, W. Tan, Evaluation of composition and crosslinking effects on collagen-based composite constructs, Acta Biomater. 6 (2010) 1413–1422.